# Role of Flow Inertia in Aggregate Restructuring and Breakage at Finite Reynolds Numbers

Akash Saxena, Jean-Sébastien Kroll-Rabotin, R. Sean Sanders

▶ **To cite this version:**

Akash Saxena, Jean-Sébastien Kroll-Rabotin, R. Sean Sanders. Role of Flow Inertia in Aggregate Restructuring and Breakage at Finite Reynolds Numbers. Langmuir, 2023, 10.1021/acs.langmuir.3c01012 . hal-04162468

**HAL Id: hal-04162468**

**https://hal.univ-lorraine.fr/hal-04162468v1**

Submitted on 14 Jul 2023

**HAL** is a multi-disciplinary open access archive for the deposit and dissemination of scientific research documents, whether they are published or not. The documents may come from teaching and research institutions in France or abroad, or from public or private research centers.

L'archive ouverte pluridisciplinaire **HAL**, est destinée au dépôt et à la diffusion de documents scientifiques de niveau recherche, publiés ou non, émanant des établissements d'enseignement et de recherche français ou étrangers, des laboratoires publics ou privés.

Copyright

# Role of Flow Inertia in Aggregate Restructuring and Breakage at Finite Reynolds Numbers

Akash Saxena,[†] Jean-Sébastien Kroll-Rabotin,[*,‡] and R. Sean Sanders[*,†]

[†]*University of Alberta, Department of Chemical and Materials Engineering Edmonton, T6G 1H9, Canada*

[‡]*Institut Jean Lamour, Université de Lorraine, CNRS, IJL, Labex DAMAS F-54000 Nancy, France*

E-mail: jean-sebastien.kroll-rabotin@univ-lorraine.fr; ssanders@ualberta.ca

**Abstract**

Forces acting on aggregates depend on their properties such as size and structure. Breakage rate, stable size and structure of fractal aggregates in multiphase flows are strongly related to the imposed hydrodynamic forces. While these forces are prevalently viscous for finite Reynolds number conditions, flow inertia cannot be ignored, thereby requiring one to fully resolve the Navier-Stokes equations. To highlight the effect of flow inertia on aggregate evolution, numerical investigation of aggregate evolution in simple shear flow at finite Reynolds number is conducted. The evolution of aggregates exposed to shear flow is tracked over time. Particle coupling with the flow is resolved with an Immersed Boundary Method, and flow dynamics are solved using a Lattice Boltzmann Method. Particle dynamics are tracked by a Discrete Element Method, accounting for interactions between primary particles composing the aggregates. Over the range of aggregate-scale Reynolds numbers tested, breakage rate appears to be governed by the combined effect of momentum diffusion and the ratio of particle interaction forces to the hydrodynamic

forces. For higher shear stresses, even when no stable size exists, breakage is not instantaneous because of momentum diffusion kinetics. Simulations with particle interaction forces scaled with the viscous drag, to isolate the effect of finite-Reynolds hydrodynamics on aggregate evolution, show that flow inertia at such moderate aggregate Reynolds numbers has no impact on the morphology of non-breaking aggregates, but significantly favors breakage probability. This is a first-of-its-kind study that establishes the role of flow inertia in aggregate evolution. The findings present a novel perspective into breakage kinetics for systems in low but finite Reynolds number conditions.

# Introduction

The physics of solid-liquid suspensions are often governed by the aggregating behavior of the solid particles transported by the liquid. Consequently, aggregate properties, such as size and structure, govern the efficiency of many industrial processes, including polymer manufacturing,[1] waste water treatment,[2,3] mineral processing[4] and liquid metal treatments.[5] In these processes, aggregates are exposed to shear which directly affects their size and structure,[6–8] thus affecting the overall suspension properties such as its rheology.[9] When an aggregate is introduced in a shear flow, it restructures so that particle contacts within the aggregate balance the external action of the flow. The aggregate breaks when force equilibrium cannot be achieved. The mechanisms at play in restructuring and breakage of fractal aggregates in shear flow have been investigated extensively yielding abundant literature on the matter since 2010.[10–13] Their conclusions have been summarized in a previous article.[14] While this research focuses on shear induced breakage of aggregates, breakage rate in a dense suspension can also be impacted by other mechanisms such as collisions between aggregates,[15] deagglomeration through flow scales smaller than the aggregates in turbulent flows[16] or collective dynamics of aggregates.[17]

Many experimental studies attempted to capture these dynamics by determining the

stable size and structure of aggregates in various flow conditions such as shear, elongational or turbulent flow.[18–24] Some studies have attempted to also capture the aggregate breakage rates.[25,26] Due to the difficulty in controlling the properties of every aggregate in an experiment, and the fact that it is impossible to experimentally measure contact forces between particles when exposing (or subjecting) aggregates to shear,[23] most investigations of aggregate dynamics have been done using numerical simulations. One of the most commonly used methods has been Stokesian Dynamics (SD),[27] which solves the Stokes equation for the flow, assuming that viscous forces largely prevail. Studies with SD have provided valuable understanding of aggregate behaviour. For example, SD has shown that the stable size of broken fragments scale exponentially with the hydrodynamic stresses of the flow,[23] with the exponent depending on the structure of the parent aggregate. Consistent observations were obtained with other approaches, like the even simpler Free-Draining Approximation[28,29] or finite volume resolution of the flow[30] for low Reynolds number conditions.

Due to the intrinsic limits of SD, these results are only applicable to extremely low Reynolds numbers. In aggregation processes, finite Reynolds effects were found to have a significant impact even for Reynolds numbers as low as 0.03.[31] Therefore, flow inertia should be expected to play a significant role in aggregate breakage and restructuring even for low Reynolds number flows, and investigations with SD cannot capture such effects. Other authors[14,32,33] have studied aggregates in flows using Lattice Boltzmann Method (LBM), demonstrating the viability of the method. In this study, we have reproduced the aggregate physics that have previously been studied using SD, and additionally obtained results under finite Reynolds number conditions, where the inertial effects in the flow at aggregate scale are not negligible. This is a pioneering study in establishing the role of flow inertia, at finite Reynolds numbers, on aggregate breakage and restructuring through numerical simulations.

# Methodology

## Aggregate creation

To have a generalized representation of aggregate behaviour, the evolution of ten aggregates is investigated. An aggregate generation algorithm described in previous works[14,34] is used. The aggregates share similar morphological characteristics and are shown in Figure 1. While aggregate size is typically quantified with the radius of gyration $R_g$,[23] density is often characterized using fractal dimension $D_f$.[6] The fractal dimension $D_f$ is defined such that

$$N = S\frac{R_g}{R_p}^{D_f} = SR_g^{*D_f} \tag{1}$$

where $N$ is the number of particles in an aggregate, $R_p$ is the radius of the primary particles and $S$ is the structure factor. It is worth noting that $R_g$, in the context of aggregates, is the ratio of the second moment of mass around the center of the aggregate to the total mass. When $N$ is constant among two aggregates, a comparison of their dimensionless radius of gyration $R_g^*$ also compares their densities; thus, $R_g^*$ can be used to quantify both size and density.[14] In this study, each aggregate has an initial fractal dimension $D_f = 2.3$ and consists of 70 rigid primary spherical particles. Consequently, all aggregates share the same dimensionless radius of gyration $R_g^* = 5.27 \pm 0.04$. The values of these parameters were chosen as a balance to reduce the computational cost of simulations while still capturing the dynamic interplay of forces and aggregate structure as observed in larger aggregates. Aggregates consisting of as few as 32 particles have been found to retain their fractal nature;[13,35] that is, results obtained with aggregates comprised of 32 primary particles were applicable to larger aggregates. Therefore, results obtained with aggregates consisting of 70 particles can be confidently applied to larger aggregates.

While morphological properties, such as $R_g$ and $D_f$, characterize the shape and size of the aggregates, the particle-particle interactions are pivotal to determine their response under hydrodynamic stresses. Thus, particle-particle interactions are treated as characteristic properties of the aggregates. The interaction forces have normal and tangential

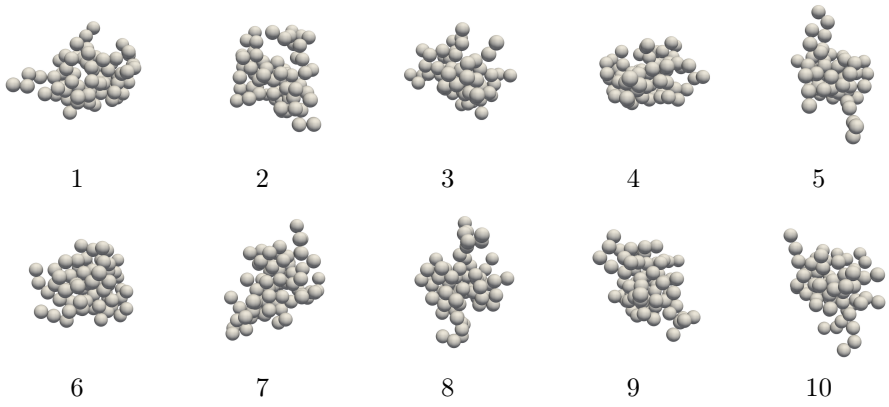


Figure 1: The 10 artificially created initial aggregates used in the simulations ($N = 70$, $D_f = 2.30 \pm 0.01$, $R_g^* \approx 5.27$).

components. The normal component combines a cohesive (attractive) force and a non-overlapping (repulsive) force. Together, they give a maximum attractive force between two particles in close contact. This maximum attractive force must be overcome to break the "bond" between any two adjacent particles within the aggregate. In this study, the cohesive forces are modeled as the van der Waals forces,[36] while the repulsive forces are modeled using Born repulsion[37] as presented in more details in Saxena et al.[14] As illustrated in Figure 2, due to the combination of an attractive force with a steeper repulsive force, a maximum cohesive force appears at $6.1 \cdot 10^{-4} R_p$ in the presented simulations, that is close enough to the particle surface to neglect it compared to other length scales in this problem. The value of this maximum is the strength of the bond, which can be controlled by setting the Hamaker constant, that is noted $A_H$ in Figure 2 and that acts a numerical parameter in the simulations. Moreover, the inclusion of tangential forces between particles allows them to resist external bending through a reactionary bending moment.[38]

The normal force steeply reduces to about $1/1000^{\text{th}}$ of its maximum value by $\approx 0.01 \times R_p$. The tangential force reaches its maximum value at an angular displacement of $\approx 0.04$ rad after which the bond is considered broken. Therefore, the distance at which both force components are non-negligible is not a parameter of interest; it is only the maximum values of these forces that influence aggregate evolution, and the origin of these forces is of little consequence. In other words, the results obtained from ag-

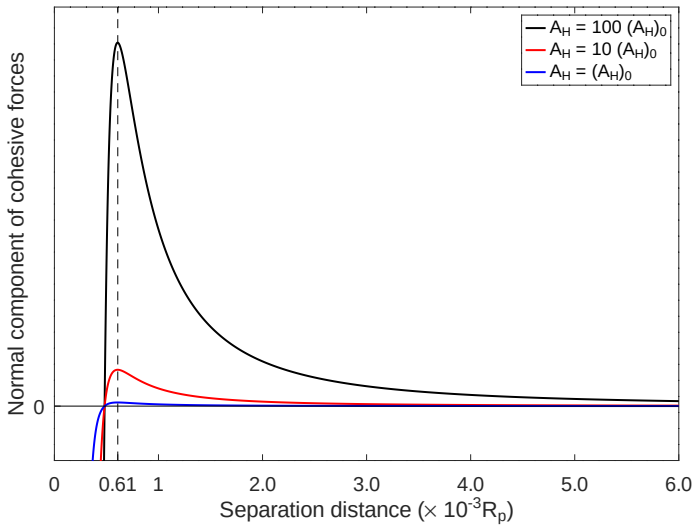


Figure 2: Normal component of the force imposed between primary particles (positive values correspond to attraction and negative to repulsion) as a function of the distance between the surfaces of the two interacting particles.

gregate studies with a particular short-ranged particle-particle interaction model will be applicable to aggregates with other types of short-range interactions. Hence, only the maximum tangential and normal forces are considered in the characterization of internal interactions.[14,30] More details on the modeling and implementation of these forces are given in previous works.[14,34]

## Numerical schemes

The evolution of an aggregate in shear flow is driven by the local hydrodynamics. To compute the hydrodynamics correctly, the flow must be resolved. Essentially, the flow around the aggregate transfers momentum to each primary particle; thus, each particle experiences inter-particle forces, and hydrodynamic forces. To allow for dynamic evolution of an aggregate in shear flow, the motion of each particle of the aggregate is tracked and updated over time. The dynamics of each particle are determined by solving Newton's laws of motion while accounting for all forces and torques acting on every particle, and trajectory integration, performed through a second order Adams-Bashforth scheme, updates the particle position. In this work, we have used a Lattice Boltzmann Method to solve the flow dynamics, an Immersed Boundary Method for two way coupling between

the fluid and each particles, and a Discrete Element Method for particle tracking. Details of these schemes can be found in previous works.[14,34]

## Simulation setup

A free-to-move aggregate is placed at the center of a cubic domain, as shown in Figure 3. The domain size is $H^3 = 198 \times 198 \times 198$ lattice units, and the radius of primary particles, $R_p$, is 5 lattice units. This allows the particles to be sufficiently discretized for the flow as discussed in Saxena[39], Chapter 3. Flow is induced by applying a constant shear stress $\tau$ at the top and bottom walls of the domain (represented by the green planes in Figure 3). The other boundaries are assigned periodic conditions. This yields a ratio $R_p/H = 0.0505$, and the overall size of aggregates estimated from their initial radius of gyration $R_g$ is 26.35 lattice units, yielding a ratio $R_g/H = 0.1331$. The aggregates are thus much smaller than the domain size, so that the hydrodynamic stresses acting on aggregates are controlled by the imposed shear stress and are not significantly affected by confinement.

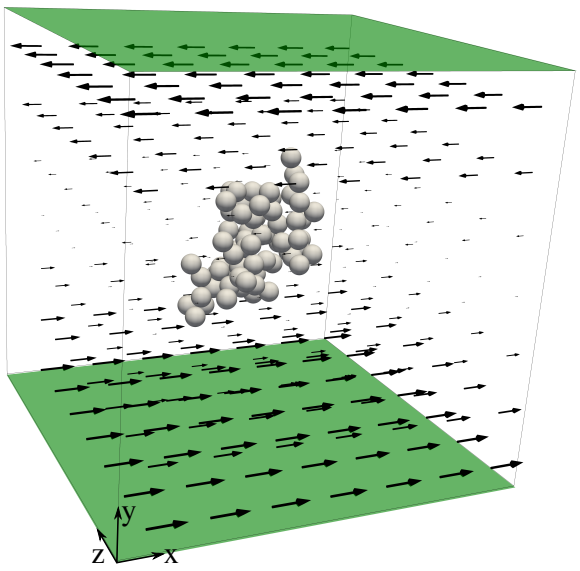


Figure 3: Simulation setup, with Aggregate 7 placed at its center: green planes represent the surfaces where shear stress is applied, and arrows show the resulting flow velocity.

Since the fluid and aggregate are initially at rest, the time taken for the flow to develop must be considered. The shear stresses $\tau$ applied on the top and bottom walls

of the domain generate momentum, which diffuses from the shear planes towards the domain center resulting in flow development. Therefore, the flow development time is essentially the time needed for momentum to diffuse through the domain. This can be estimated by considering a 1D momentum diffusion equation:

$$\frac{\partial u}{\partial t} = \nu \frac{\partial^2 u}{\partial y^2} \tag{2}$$

where $\nu$ is the kinematic viscosity, $y$ is the direction normal to the shear-imposed planes and $u$ is the local velocity in the flow. An order-of-magnitude analysis of Equation (2) allows us to quantify the diffusion time $t_d$ as

$$t_d \equiv \frac{(h/2)^2}{\nu} \tag{3}$$

where $h$ is the size of the domain. A non-dimensional diffusion time can be defined as

$$t_d^* = \dot{\gamma} t_d \tag{4}$$

where $\dot{\gamma}$ is the shear rate in the flow resulting from the imposed shear stresses at domain boundaries, defined as

$$\dot{\gamma} \equiv \frac{\tau}{\rho \nu} \tag{5}$$

where $\tau$ is the imposed shear stress, $\rho$ is the fluid density and $\nu$ its kinematic viscosity.

Numerical solution of Equation (2) shows that at $t_d^* = 1$, the shear rate at the center of the domain reaches 90% of the value imposed at the boundaries.

## Quantification of flow conditions and aggregate properties

The shear rate, $\dot{\gamma}$, as defined in Equation (5) is the target shear rate, which corresponds to the shear stresses applied at the top and bottom boundaries. Using this definition, the resulting flow conditions at the aggregate scale can then be characterized as

$$\mathrm{Re}_{\mathrm{agg}} = \frac{\dot{\gamma}\ (2R_g)^2}{\nu} = \frac{4\tau R_g^2}{\rho \nu^2}. \tag{6}$$

As an aggregate evolves and restructures, its radius of gyration $R_g$ changes, leading to a change in its $\mathrm{Re}_{\mathrm{agg}}$ as well. To reduce the complication of a dynamically varying aggregate Reynolds number, analyses were performed with the initial aggregate Reynolds number, based on the initial radius of gyration for the aggregate $R_{gi}$:

$$\mathrm{Re}_{\mathrm{agg}}^{\mathrm{init}} = \frac{4\tau R_{gi}^2}{\rho\nu^2}. \tag{7}$$

While $\mathrm{Re}_{\mathrm{agg}}$ captures the flow physics at aggregate scale, the dynamics at the scale of primary particles can be quantified with a particle Reynolds number:

$$\mathrm{Re}_{\mathrm{p}} = \frac{4\tau R_p^2}{\rho\nu^2} \tag{8}$$

where $R_p$ is the radius of the primary particles. Note that $\mathrm{Re}_{\mathrm{p}}$ is independent of aggregate properties.

While each Reynolds number corresponds to a constant hydrodynamic stress $\tau$, the response of an aggregate to hydrodynamic forces also depends on the inter-particle cohesive and tangential forces. Such forces are thus considered to be characteristic properties of aggregates. More precisely, the maximum values of these forces determine the evolution of the aggregates.[30] In this study, the inter-particle forces are modeled with a normal cohesive component and a tangential component. Since inter-particle forces and hydrodynamic forces compete with each other, the ratio of these two competing forces forms a dimensionless parameter which characterizes the strength of the inter-particle bonds against the hydrodynamic forces. Therefore, the two components of the inter-particle forces, $F_n^*$ and $F_t^*$, are normalized by the hydrodynamic forces $F_{drag}$ estimated through Stokesian drag. This can be represented as

$$F_n^* = \frac{F_n}{F_{drag}} = \frac{F_n}{12\,\pi\,\rho\nu\,R_p^2\,\dot{\gamma}} \tag{9}$$

$$F_t^* = \frac{F_t}{F_{drag}} = \frac{F_t}{12\,\pi\,\rho\nu\,R_p^2\,\dot{\gamma}} \tag{10}$$

where $F_n$ and $F_t$ are the maximum normal and tangential forces attainable between any

two particles in close contact, while the drag force $F_{drag}$ is estimated using the maximum difference of Stokesian drag between two bonded primary particles.

### Breakage detection

The bond between two adjacent particles in an aggregate can be considered to be broken when the distance between them is such that cohesive forces are small compared to the maximum cohesive forces. Since van der Waals forces are inversely proportional to the square of the surface to surface distance, the cohesive forces are negligible at $0.1R_p$. Although this criterion is quite large compared to that of Harshe and Lattuada [13] ($\approx 0.001$ $R_p$), it allows for the possibility that particles may reattach, which is realistic in shear flow. For this work, a breakage event is said to have occurred when two or more groups of particles (fragments) are separated by at least 0.1 $R_p$.

## Results and discussion

An isolated aggregate in shear flow is likely to either restructure or break. Although both outcomes are driven by the hydrodynamic forces, the responsible physical mechanisms are different. The breakage is mostly associated with the strength of the cohesive bonds and the rigidity of the aggregate, whereas restructuring is known to be mainly dependent on the bending moment in the aggregate. [14] When the flow has non-negligible inertia, the Reynolds number adds a new degree of freedom to the physical problem of aggregate restructuring and breakage.

### Evolution of size and breakage rate with shear rate at finite Reynolds number

To highlight the role of flow inertia on aggregate evolution, simulations are performed for aggregate Reynolds numbers $\mathrm{Re}_{\mathrm{agg}}^{\mathrm{init}}$ ranging from 0.4 to 10. In such conditions, inertial flow patterns start to appear at aggregate scale. In contrast, the corresponding particle Reynolds numbers, $\mathrm{Re}_{\mathrm{p}}$, vary from 0.0143 to 0.3587, implying that the inertial effects

at primary particle scale remain comparatively low. The two Reynolds numbers are related by the dimensionless initial radius of gyration of aggregates: $\mathrm{Re_p} = \mathrm{Re_{agg}^{init}}/{R_{gi}^*}^2$. Since both Reynolds numbers depend on the shear rate, they are controlled by imposing shear stresses at boundaries. Physically, this simulation plan is equivalent to exposing each aggregate to different Reynolds number conditions in the same fluid, by varying the shear.

**Aggregate fragmentation**

Each simulation begins with the aggregate at rest, while flow is induced through shear stresses at the top and bottom boundaries (Figure 3). As the flow diffuses towards the center of the domain, the aggregate starts to evolve. The morphological properties of the aggregate ($R_g$ or $D_f$) are recorded over a period of $80\,\dot{\gamma}^{-1}$ or until it breaks, whichever comes first. The stable radius of gyration for the simulated conditions has been defined as the radius of gyration reached by the aggregates that do not break at the end of the $80\,\dot{\gamma}^{-1}$. If aggregates break into fragments before the end of the simulation, their breakage time $t_{\mathrm{break}}$ as well as the sizes $R_g$ of each broken fragment are recorded.

Under the conditions of this study, 2 of the 10 aggregates broke at $\mathrm{Re_{agg}^{init}} = 0.4$, 9 aggregates broke at $\mathrm{Re_{agg}^{init}} = 0.8$, and all 10 aggregates broke for all other $\mathrm{Re_{agg}^{init}}$. It can therefore be concluded that aggregates are mostly stable in low Reynolds number conditions. As shown by Saxena et al.,[14,34] aggregate survival depends on whether the cohesive forces between particles can resist the drag force acting on a series of particles rather than on isolated particle pairs. Considering that the aggregates were stable at $\mathrm{Re_{agg}^{init}} = 0.4$, the force ratios $F_n^*$ and $F_t^*$ were determined from Equations (9) and (10) as

$$F_n^* = F_t^* = \frac{F_n}{12\pi\,\rho\,\nu\,R_p^2\,\dot{\gamma}} \tag{11}$$

$$= \frac{F_n}{3\pi\,\rho\,\nu^2\frac{0.4}{R_{gi}^*}} = \frac{F_n}{3\pi\,\rho\,\nu^2\;0.0143} \tag{12}$$

$$\Rightarrow F_n^* = F_t^* = 7.395 \tag{13}$$

These force ratios at $\mathrm{Re_{agg}^{init}} = 0.4$ are henceforth referred to as $(F_n^*)_{\mathrm{stable}}$.

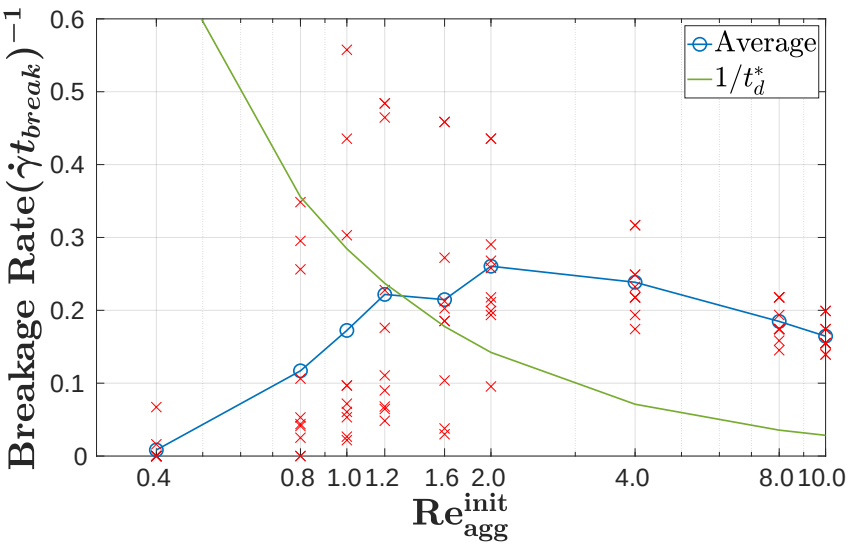


Figure 4: Breakage rate of the 10 initial aggregates at various Reynolds numbers. Crosses (×) mark individual aggregates while the average rate for all the broken aggregates is plotted as circles joined by a continuous line (–).

Figure 4 shows the breakage rate, calculated as the inverse of the dimensionless breakage time $\dot{\gamma}t_{\text{break}}$, of the 10 initial aggregates as a function of their initial aggregate Reynolds number $\text{Re}_{\text{agg}}^{\text{init}}$. The breakage rate is found to increase in low Reynolds number conditions ($\text{Re}_{\text{agg}}^{\text{init}} < 1.6$). At these low Reynolds numbers, hydrodynamic forces are predominantly viscous. When Reynolds number is increased by increasing the shear rate, the hydrodynamic forces increase proportionally. With increasing hydrodynamic forces, the force ratios decrease and eventually become smaller than $(F_n^*)_{\text{stable}}$, and aggregates are thus expected to break more quickly. This trend of increase in breakage rate for $\text{Re}_{\text{agg}}^{\text{init}} < 1.6$ is consistent with the findings of Harshe and Lattuada [13], where breakage rate was observed to increase with shear rate. However, for values of $\text{Re}_{\text{agg}}^{\text{init}}$ above 1.6 ($\text{Re}_{\text{p}} < 0.0574$), the dimensionless breakage rate stops increasing, and even tends to gradually decrease.

To explain this observed change in behavior at $\text{Re}_{\text{agg}}^{\text{init}} = 1.6$, a combined effect of two factors must be noted: (i) low cohesive to drag force ratio, and (ii) the time taken for the momentum to diffuse from the boundary to the aggregate. When the cohesive to drag force ratio is small enough for the aggregates to break instantaneously, the breakage rate is governed only by the time taken for the hydrodynamic forces to develop around the aggregate. At $\text{Re}_{\text{agg}}^{\text{init}} = 1.6$, the cohesive forces are too weak to balance the hydrodynamic

forces: the ratio at this critical Reynolds number of 1.6 can be calculated from Equations (9) and (10). It can be seen that the forces ratios reduce to 0.25 $(F_n^*)_{\text{stable}}$; that is, the hydrodynamic forces are effectively four times stronger than the inter-particle bonds. Under such conditions, the hydrodynamic stresses are too strong for the aggregate's cohesive forces to counter-balance. This results in definite breakage of the aggregates without any restructuring. However, since it takes some time for the flow to develop from the boundaries and reach the aggregate, the breakage is not instantaneous (that is, breakage rate is not infinite). This momentum diffusion from the boundary to the center of the domain scales with the diffusion time $t_d^*$ defined in Equation (4). As a result, when the hydrodynamic driving forces are too strong relative to cohesive forces within aggregates, breakage rate becomes a function of the diffusion time instead of the shear rate. This becomes evident when the dimensionless breakage rate is compared to the similarly constructed diffusion rate defined as the inverse of the dimensionless diffusion time $(1/t_d^*)$. It is plotted along with the breakage rate for corresponding Reynolds numbers in Figure 4, which shows that once the critical force ratio is reached at $\text{Re}_{\text{agg}}^{\text{init}} = 1.6$ ($\text{Re}_{\text{p}} = 0.0574$), breakage rate is governed by the diffusion time instead of the shear rate.

To conclude, diffusion time, rather than shear rate, is found to govern the breakage rate of weak aggregates; that is, when the breakage time of aggregates is bounded by the momentum diffusion time in the flow. Such conditions may arise when an aggregate undergoes sudden large variations in flow conditions, for example, in turbulent flow. In contrast, breakage rate scales with shear rate when breakage is governed by the force ratios instead of diffusion time, resulting in aggregates evolving over time and restructuring until they break or reach stable configurations.

### Breakage mechanism

A statistical analysis of fragment size distributions was attempted to highlight any difference in the underlying breakage mechanisms. Specifically, fragment sizes were compared between breakage with and without restructuring, such as erosion versus fragmentation. Erosion can be defined as detachment of a few particles from the aggregate, whereas

breakage through fragmentation results in formation of smaller aggregates of comparable sizes. The analysis showed no difference in breakage behaviour, implying that the fragmentation dynamics at play were similar for all flow conditions considered. This is due to the fact that although the Reynolds numbers of interest in this study are finite, they are still low. Therefore, the whole aggregate experiences shear forces that remain of similar magnitude between their core and their shell. In the end, there is no significant difference with breakage in a fully developed shear flow. Figure 5 presents examples of fragments from two aggregates (Aggregate 4 and 5 from Figure 1) and shows that large or small fragments can form at any Reynolds number, with or without significant restructuring before breakage.

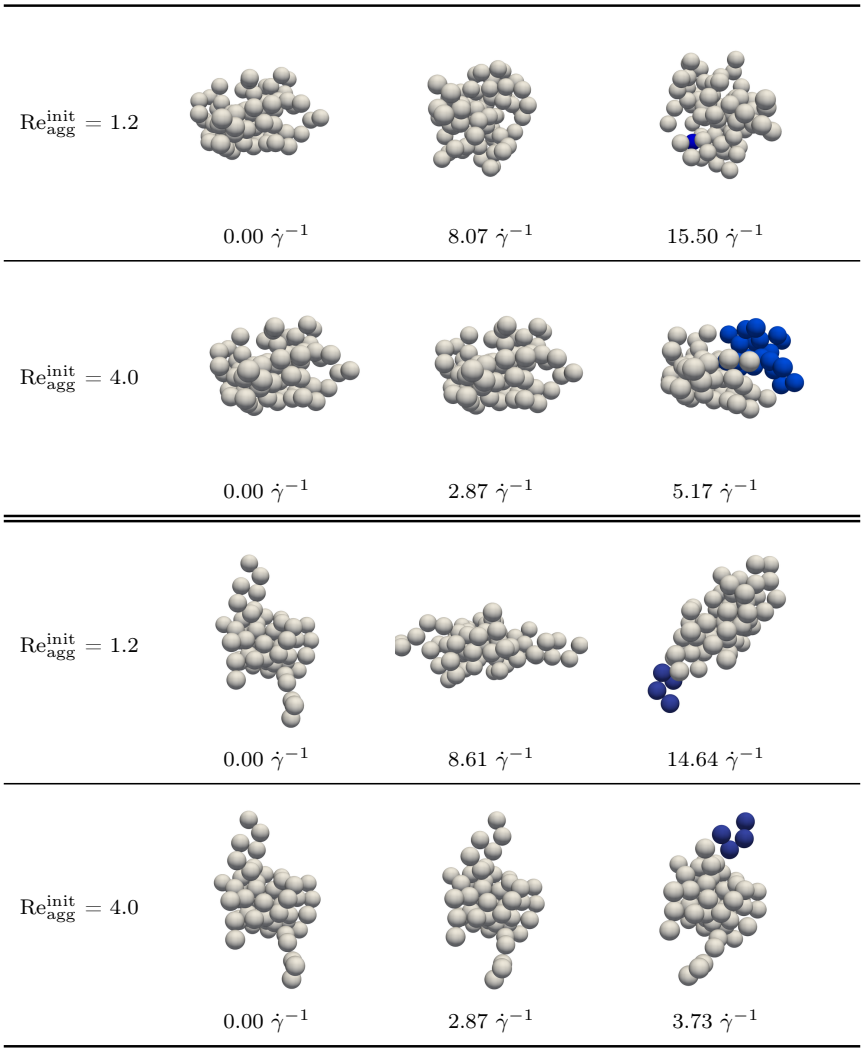


Figure 5: Example of evolution over time of two aggregates (top: Aggregate 4, bottom: Aggregate 5 from Figure 1) at different Reynolds numbers. Broken fragment is highlighted in blue.

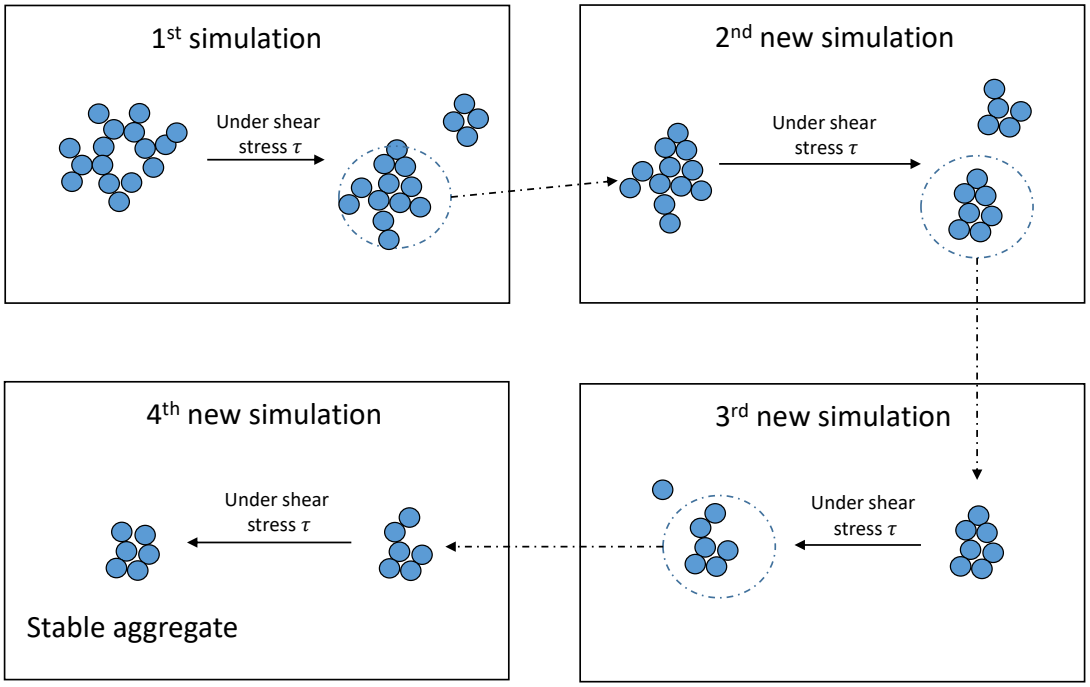


Figure 6: Tracking of aggregate evolution through restructuring and breaking: the largest fragment is selected and studied separately under similar flow conditions.

### Breakage cascade and stable size

To determine the largest stable size for the flow conditions considered, the largest fragment of the broken aggregate is selected and reintroduced into a new simulation; i.e., with shear stresses at top and bottom boundaries and zero initial velocity in the domain. The shear stresses are kept constant between the domain where the fragment was formed and in the new domain. Since the new aggregate is smaller, the new simulation has a lower aggregate Reynolds number. Nonetheless, $\mathrm{Re_p}$ remains constant. This process of selecting the largest broken fragment is repeated up to seven times, or until a stable configuration is reached. Figure 6 graphically illustrates this breakage cascade. At the end of the first simulation, the largest of the broken fragments is selected and its evolution is simulated under the same shear stress $\tau$ at the boundaries as first simulation, with both the flow and the aggregate intially at rest.

Figure 7 shows the breakage rate of initial aggregates and all subsequent fragments at different shear rates as a function of the size $R_g^*$. Since fragments have varying sizes, their aggregate Reynolds numbers cannot be used to represent the action of shear. Instead, force ratio as defined in Equation (9) is used. For any given force ratio, all aggregates at

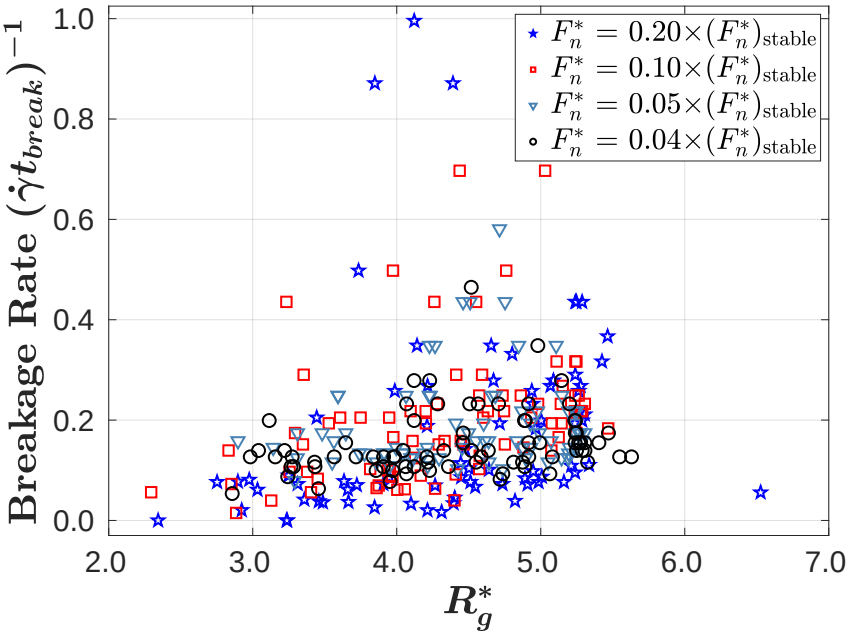


(a) Breakage rate for $\text{Re}_{\text{agg}}^{\text{init}} > 1.6$

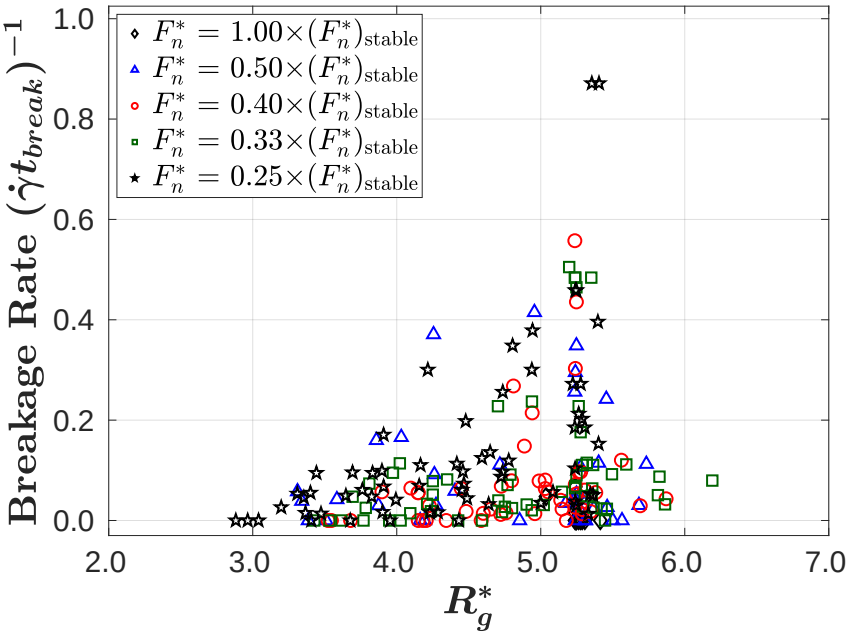


(b) Breakage rate for $\text{Re}_{\text{agg}}^{\text{init}} \leq 1.6$

Figure 7: Breakage rate of aggregates and subsequent largest fragments from the breakage cascade, (a) all aggregates and fragments with $\text{Re}_{\text{agg}}^{\text{init}} > 1.6$, that is, with $F_n^* < 0.25\ (F_n^*)_{\text{stable}}$, (b) aggregates and fragments with $\text{Re}_{\text{agg}}^{\text{init}} \leq 1.6$, that is, with $F_n^* \geq 0.25\ (F_n^*)_{\text{stable}}$.

the beginning of the breakage cascade are of similar size ($R_g^* \approx 5.27$). If the aggregate breaks, its breakage rate is plotted against its size at breakage. Following the breakage cascade, the breakage rate of the subsequent larger fragments are plotted against their size at breakage. If the aggregate or the fragment did not break, a breakage rate of 0 is plotted against its final stable size. To extract a trend, datasets are presented separately according to the two groups of breakage kinetics presented in Figure 4, that is $F_n^* < (F_n^*)_{\text{stable}}$ (Figure 7a) and $F_n^* \geq (F_n^*)_{\text{stable}}$ (Figure 7b). Dividing the data into these two categories enables distinction of breakage kinetics for a range of aggregate sizes between diffusion time and force ratio dominated breakage mechanism.

In Figure 7a, the breakage rate is quasi-exclusively non-zero. No stable size is observed in such conditions: only small fragments hold together, and these fragments contain too few primary particles (much less than 32 primary particles) to be treated as fractal objects. The breakage rate shows little correlation with aggregate size, and no dependence on force ratio. It must be mentioned that although larger aggregates do break slightly faster, their breakage rates are widely scattered and since hydrodynamic forces prevail for all aggregates in this figure (that is, $F_n^* < (F_n^*)_{\text{stable}}$), they can break regardless of the strength of the cohesive forces.

Figure 7b shows that when the breakage rates are lower than the rate of flow diffusion $1/t_d^*$, at $\text{Re}_{\text{agg}}^{\text{init}} \leq 1.6$, breakage dynamics are governed by the force ratios. Under these conditons, the breakage rate correlates quite well with the size of the fragment. All the force ratios presented in Figure 7b yield a breakage rate of zero after the breakage cascade; that is, by the end of the breakage cascade, all aggregates break into fragments that do not break. The size corresponding to breakage rate of zero is the stable $R_g^*$ for the respective force ratio (or, for the respective shear stresses). This confirms that most aggregate fragments reach a stable size, and that this stable size depends on the hydrodynamic shear stress. To reach this stable size, some aggregates undergo multiple fragmentation stages, while others are stable at much larger sizes. For example, at $F_n^* = 0.5 \times (F_n^*)_{\text{stable}}$, one of the aggregates from Figure 1 underwent 5 fragmentations to reach a stable size of $R_g^* = 3.65$, whereas another underwent breakage only once and the fragment

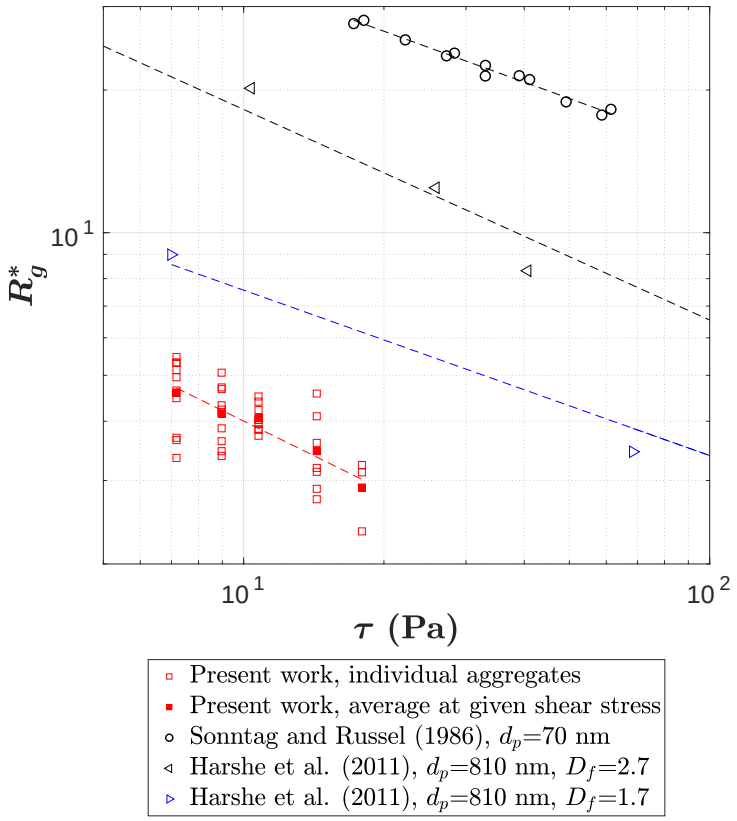


Figure 8: Stable size of fragments under different shear conditions compared to other studies.

with a size of $R_g^*$= 5.23 was found to be stable. For high enough force ratios, some of the initial 10 aggregates appear to be stable; that is, they restructure but do not break at all. Hence some points with breakage rate equal to zero correspond to radii of gyration very close to the initial aggregates (some even a little larger). By the end of the breakage cascade, a stable size was found for most aggregates at $\mathrm{Re}_{\mathrm{agg}}^{\mathrm{init}} \leq 1.6$. Overall, smaller aggregates are observed to have a lower breakage rate due to lower hydrodynamic forces at aggregate scale.

As previously discussed and as illustrated in Figure 5, the nature (mechanism) of the fragmentation does not seem to be impacted by the range of Reynolds numbers considered in this study. Therefore, the correlation of the stable size with shear rate remains consistent with the observations from other studies where fragmentation at low Reynolds numbers was investigated. Figure 8 shows the scaling of stable size with the shear stress $\tau$ collected from several studies, where the largest stable size $R_g^*$ has been reported to scale as $R_g^* \propto \tau^{-p}$. To compare with the literature, the stable size determined

through the breakage cascade for the investigated flow conditions is also presented in Figure 8. For this comparison, the simulation data had to be converted to physical values by assuming fluid properties, cohesive forces and particle size. Considering water properties for the fluid, the data in Figure 8 uses the following conditions for particles:

$$F_n = 1 \times 10^{-9} \text{ N} \qquad\qquad R_p = 1 \times 10^{-6} \text{ m}$$

The shear stresses in the flow are estimated from Equation (7) as:

$$\tau = \frac{\text{Re}_{\text{agg}}^{\text{init}} F_n}{4 \left(R_p R_{ig}^*\right)^2}$$

Most aggregates did not break at $\text{Re}_{\text{agg}}^{\text{init}} = 0.4$, which reflects that the largest stable size is likely to be larger than the aggregates investigated in the study. Therefore, points at $\text{Re}_{\text{agg}}^{\text{init}} = 0.4$ are not represented in Figure 8.

Table 1: Scaling exponents reported in literature for stable size dependence on hydrodynamic shear stress.

| Exponent, $p$ $R_g^* \propto \tau^{-p}$ | Literature | Conditions | Simu. | Exp. |
|---|---|---|---|---|
| 0.35 | Eggersdorfer et al. [28] | Low Reynolds | FDA | |
| 0.35 | Sonntag and Russel [18] | Low Reynolds | | ✓ |
| 0.35 to 0.55 | Harshe et al. [23] | Low particulate Reynolds, experiments up to turbulence | SD | ✓ |
| 0.48 | Kroupa et al. [30] | Low Reynolds | FV | |
| 0.48 | *Present work* | Laminar, Finite Reynolds | LBM | |
| 0.5 | Ehrl et al. [21] | Turbulent, low particulate Reynolds | | ✓ |
| 0.5 | Bouyer et al. [40] | Turbulent, low particulate Reynolds | | ✓ |
| 0.52 | Zaccone et al. [41] | Laminar and turbulent, low particulate Reynolds | | ✓ |
| 0.6 | Saha et al. [26] | Turbulent, low particulate Reynolds | | ✓ |

The value of the exponent $p$ fitting the data presented in this current work is 0.48, which compares well to values reported in the literature, which range from 0.35 to 0.55.[18,21,23,28,30,41] Saha et al.[26] reported a value $p = 0.6$ in turbulent conditions with aggregate size larger than the Kolmogorov length scale. Table 1 reports the values from these studies. It must be pointed out that the final fractal dimension $D_f$ of the stable

fragments from this work ranges between 2.1 and 2.4, whileHarshe and Lattuada [35] predicts $D_f = 2.4$. The difference could be due to the geometrical limitation in achieving a high fractal dimension for smaller fragments: when an aggregate consists of too few particles, the scaling exponent of mass with size (that is, the fractal dimension) cannot reach high values even with closely packed aggregates.

To summarize the findings presented so far, when an aggregate is exposed to a Reynolds number which scales with the system's shear rate, the breakage rate stops being a function of aggregate size and shear stresses beyond some critical shear. This happens once the hydrodynamic forces are too large compared to cohesive forces. Under such conditions, breakage rate instead is scaled by momentum diffusion in the flow. It is worth mentioning that since the diffusion time depends on the size of the domain, it is here imposed by the simulation setup. In real conditions, it is a process dependent parameter. Overall, the restructuring and breakage of aggregates under shear in finite Reynolds conditions depend on two parameters, the diffusion time and the force ratios $F_n^*$ and $F_t^*$.

In the data presented so far, the Reynolds number is varied through the shear rate in the flow. Therefore, both the force ratios and diffusion time vary when different Reynolds numbers are investigated. This makes it impossible to distinguish their relative impact on aggregate behaviour independently from each other. The approach described in the next section overcomes this limitation.

## Distinguishing the effect of flow inertia from cohesive to drag force ratios

### Approach

The previous section shows that both the force ratios and finite Reynolds number flow dynamics play a role in morphological evolution and breakage of aggregates. However, the two phenomena were coupled in the previous section: an increase in Reynolds number also led to a change in force ratios, resulting in aggregate evolution under the combined

effect of force ratio and finite Reynolds dynamics. While one of the effects of flow inertia was observed as delaying breakage due to diffusion time, its effect on hydrodynamic forces was not identified. One way to distinguish this is by keeping the force ratios constant over a range of Reynolds number conditions. Thus, in this second analysis, the cohesive and tangential forces are scaled with Reynolds number such that their dimensionless forces ratios remain constant within a given dataset. Furthermore, the scaled values of the forces can be chosen to favor restructuring or breakage. Particularly, tangential forces are varied as they are known to make aggregates brittle[14] resulting in less restructuring and therefore a higher probability of breakage. Aggregate evolution studies performed at very low Reynolds number have shown that high tangential forces induce less restructuring[14,42] but more breakage.[14] This information is leveraged to investigate the effect of flow inertia on aggregate evolution. Particularly, evolution of aggregates with high tangential forces is investigated in finite Reynolds number conditions to highlight the role of flow inertia on breakage. Conversely, the effect of flow inertia on restructuring is studied by exposing aggregates with low tangential forces (aggregates more likely to restructure) to different Reynolds number conditions. The following conditions are considered:

$$\begin{aligned} F_n^* &= (F_n^*)_{\text{stable}} = 7.395, \\ F_t^* &\in \{0.01, 0.10, 1.00\} \times F_n^*. \end{aligned} \tag{14}$$

While the effect of force ratios under very low Reynolds number conditions has been widely reported in the literature,[12,14,42–46] it has not been extensively investigated in finite Reynolds number conditions. Among the few studies at finite Reynolds numbers, Saha et al.[26] considered the impact of different constituents of hydrodynamic stresses such as turbulent shear, normal and drag forces on aggregate breakage in turbulent conditions. Despite their attempt to account for hydrodynamic stresses, relative contribution of inter-particle interactions has still not been well examined at finite Reynolds numbers.

The same ten aggregates presented in Figure 1 are considered and the maximum cohesive force $F_n$ is set to 7.395 times the Stokesian drag at each Reynolds number tested. Since the probability of breakage and the extent of restructuring are controlled by the

tangential force ratio $F_t^*$, values of $F_t^*$ from 0.01 $F_n^*$ to 1.00 $F_n^*$ are considered, as stated in Equation (14). The aggregate Reynolds number ($\mathrm{Re}_{\mathrm{agg}}^{\mathrm{init}}$), on the other hand, varies from 0.4 to 40. To ensure that the aggregates experience the hydrodynamic forces imposed on the domain, the time taken for the flow to develop (that is, the diffusion time) must be kept small compared to the overall duration of the simulation. However, this is not always practical as a high $t_d^*$ may require long simulations which can be computationally expensive. Therefore, for each $\mathrm{Re}_{\mathrm{agg}}^{\mathrm{init}}$ considered, the simulation duration has been kept as large as practical compared to the corresponding diffusion time $t_d^*$. The duration of the simulated period (expressed as dimensionless strain) along with other simulation parameters are listed in Table 2.

Table 2: Dimensionless flow diffusion times $t_d^*$ and simulation duration (expressed as total strain $\dot{\gamma}t$) for the tested Reynolds numbers.

| Reynolds number $\mathrm{Re}_{\mathrm{agg}}^{\mathrm{init}}$ | diffusion time $t_d^*$ | total duration $\dot{\gamma}t$ |
|---|---|---|
| 0.4 | 1.41 | 80 |
| 1.0 | 3.52 | 120 |
| 4.0 | 14.1 | 200 |
| 10 | 35.2 | 500 |
| 40 | 140. | 700 |

Figure 9 presents the time evolution of $R_g^*$ as a function of of $\mathrm{Re}_{\mathrm{agg}}^{\mathrm{init}}$. Figure 9a shows case $F_t^* = 1{\times}F_n^*$, in which most aggregates are expected to break. Figure 9b shows case $F_t^* = 0.1{\times}F_n^*$, in which some aggregates are expected to break while some are expected to only restructure. Figure 9c shows case $F_t^*{=}0.01{\times}F_n^*$, where the least breakage is expected. As expected, some aggregates break while some attain a stable configuration. The aggregates that do not break by the end of the simulated period are assumed unlikely to break even if the simulations were run for longer durations (more justification for this assumption is discussed in Section ). In the figure, continuous lines show the evolution of the averaged $R_g^*$ of non-breaking aggregates. The corresponding confidence interval (calculated as the standard error around that average) is represented as a colored area of the same hue. For example, in Figure 9b, the solid blue line corresponds to the averaged $R_g^*$, while the shaded area in lighter blue represents the standard error around

the averaged $R_g^*$. Aggregates that break before the end of the simulated period are neither accounted for in the average behaviour, nor in its confidence interval. Instead, they are individually represented as dotted lines and their breakage events are represented as crosses terminating their evolution curve. Moreover, the time needed for the flow to develop is indicated as a vertical line at $\dot{\gamma}t = t_d^*$ for each Reynolds number.

With the above approach, plots of Figure 9 are hereby discussed to establish the effect of Reynolds number on breakage and restructuring.

**Impact of aggregate Reynolds number on breakage**

To find a relation between aggregate breakage and flow dynamics, aggregates that are likely to break are considered. Since greater inter-particle tangential forces produce more frangible aggregates,[14] the inter-particle forces $F_t^* = 1.0 \times F_n^*$ lead to aggregate breakage. The results of these simulations are presented in Figure 9a.

Figure 9a shows that aggregates restructure and break for all Reynolds numbers except for $\mathrm{Re}_{\mathrm{agg}}^{\mathrm{init}} = 0.4$. In Figures 9b and 9c, most breakage events appear much before the end of the simulation for each Reynolds number, and the radius of gyration of non-breaking aggregates remains stable for a significant period of time. This justifies the assumption that the non-breaking aggregates found at the end of each simulation are very unlikely to break even if much longer simulations were conducted, and so have reached a stable configuration.

To summarize the effect of flow inertia on aggregate breakage, a breakage probability is defined as the ratio of the number of aggregates that broke to the total number of aggregates (10). Figure 10 establishes that the breakage probability for the $F_t^*$ values studied here increases with Reynolds number. When tangential forces are significantly smaller than normal forces $F_t^* = 0.01 \times F_n^*$ and $F_t^* = 0.1 \times F_n^*$), the breakage is primarily governed by the hydrodynamic forces and the normal force component. Consequently, the curves for the aggregates with lower tangential forces in Figure 10 are very similar, to the precision that can be obtained from a sample of 10 aggregates. This also confirms that, for a given Reynolds number, tangential forces tend to favor breakage.[14]

(a)

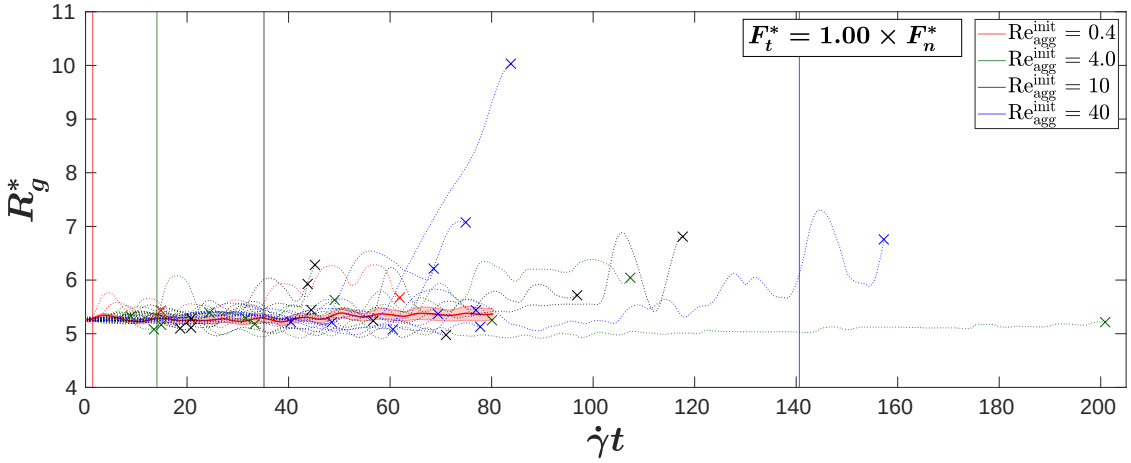


(b)

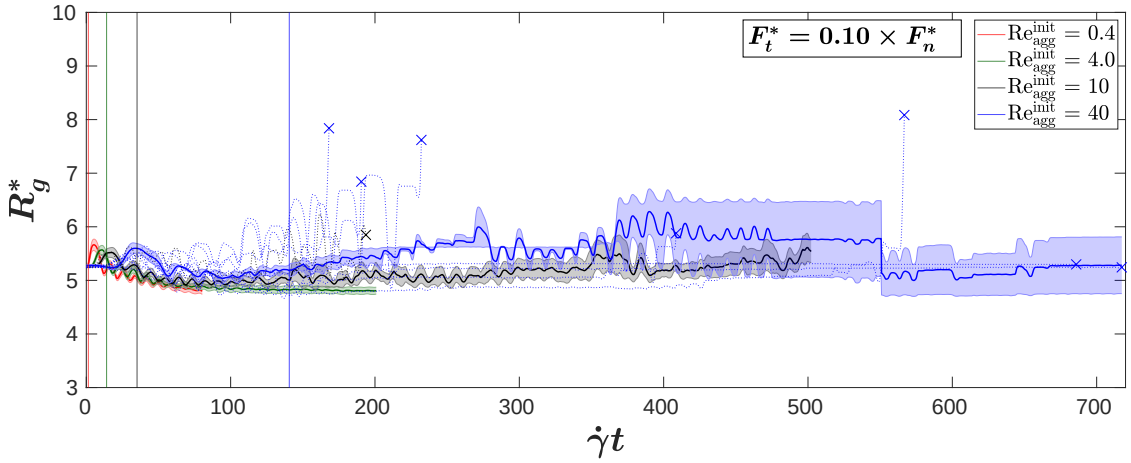


(c)

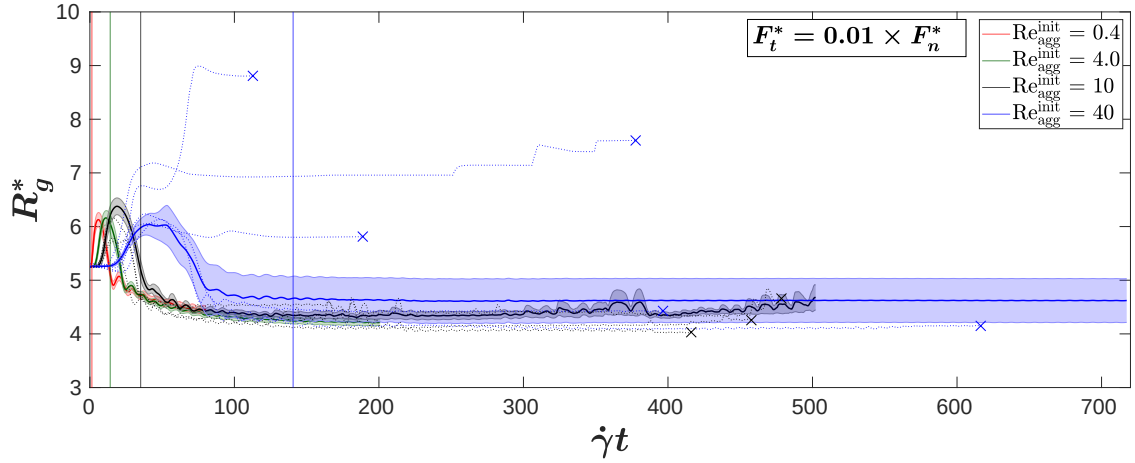


Figure 9: Evolution of aggregates over time for three different tangential force ratios (a) $F_t^* = 1.00 \times F_n^*$, (b) $F_t^* = 0.10 \times F_n^*$ and (c) $F_t^* = 0.01 \times F_n^*$. Average $R_g^*$ of non-breaking aggregates for a given shear rate and its standard error are plotted as continuous lines and shaded areas of the same color. Evolution of breaking aggregates is plotted as dashed lines (- -) and breakage events are marked with crosses (×).

Since in each plot of Figure 9 all aggregates are characterized by the same force ratios, the dependence of breakage probability on Reynolds number as shown through Figure 10 can solely be attributed to the flow inertia. The Reynolds number of primary particles $\mathrm{Re_p}$ ranges from 0.0143 to 1.4350, and thus remains too low to explain the increased breakage rate as an effect of increased drag acting on individual particles. However, aggregate scale Reynolds number is about $R_g^{*2} \sim 25$ times larger than the $\mathrm{Re_p}$, and the flow dynamics at aggregate scale start to show some non-linearities associated with finite Reynolds number effects.[47] Specifically, aggregates rotate slightly more slowly than the surrounding liquid, which is similar to the retarded rotation of a sphere at finite Reynolds numbers,[48] leading to higher shear rates around the aggregates. Additionally, the resistance to deformation of the aggregate core, which causes a flow disturbance, has previously been identified as an important mechanism that shields the particles in the aggregate shell from the shear stresses[14] of free flow. This flow disturbance dampens the strain part of the shear, which leads to aggregate shell undergoing lower compression and traction forces, resulting in less restructuring and breakage. A decrease in the relative effect of viscous contributions due to increasing Reynolds number tends to shrink the flow disturbances (in both magnitude and expanse) caused by the aggregate. This results in a decreased shielding effect, and can explain the increase in breakage rate with increasing Reynolds number.

While flow inertia is found to increase breakage probability, it is found to have no significant impact on breakage kinetics. This can be observed when dimensionless breakage time $\dot{\gamma} t_{\mathrm{break}}$ is plotted against $\mathrm{Re}_{\mathrm{agg}}^{\mathrm{init}}$. Figure 11 shows that for $F_t^* = 1.00 \times F_n^*$, the aggregates in this study tend to break at around the same strain, that is $\dot{\gamma} t = 40$, irrespective of the $\mathrm{Re}_{\mathrm{agg}}^{\mathrm{init}}$. The slightly higher dimensionless breakage times for $\mathrm{Re}_{\mathrm{agg}}^{\mathrm{init}}$ of 10.0 and 40.0 can be attributed to the delay caused by diffusion time. Since $\dot{\gamma} t$ is numerically equivalent to twice the rotation in the flow, and assuming that the aggregates rotate with the flow due to low particle inertia (primary particle Stokes number = 1/18 $\mathrm{Re_p}$), it can be deduced that the aggregates break after about 3 full rotations for $F_t^* = 1.00 \times F_n^*$. In other words, if the aggregates survive around 3 to 4 rotations ($\dot{\gamma} t = 40$ to 50), they are unlikely to break at all.

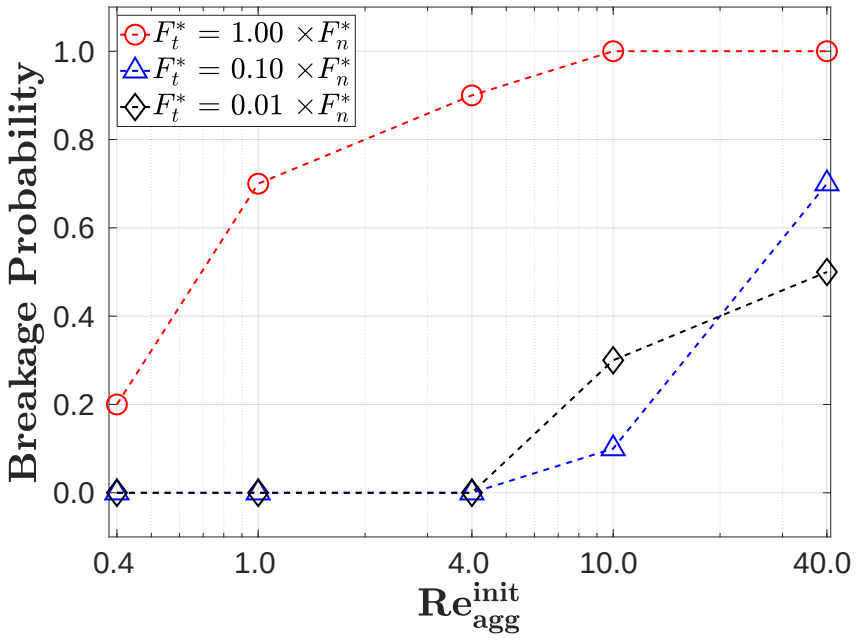


Figure 10: Aggregate breakage probability at different Reynolds numbers.

**Impact of aggregate Reynolds number on restructuring**

With respect to restructuring, there does not seem to be any relation with Reynolds number. In Figure 9, the initial differences in restructuring at different Reynolds numbers are related to the fact that momentum is still diffusing into the domain. Beyond diffusion time, aggregates restructure significantly during their first rotation to balance hydrodynamic forces with internal cohesive forces, then they break (if no balance is achieved) or reach a stable configuration, as shown by the relatively constant values over time of the average radius of gyration and of its standard error.

Although aggregates with lower tangential inter-particle forces reach denser stable configurations (smaller values of $R_g^*$) as expected from former observations,[14] their size seems independent of the Reynolds number. In Figures 9b and 9c, all continuous lines reach very similar $R_g^*$ values at the end of each simulation. This shows that non-linearities in the flow, such as reduced rate of rotation and higher shear rates around the aggregates, have little impact on determining the structure of the aggregate, at least at these moderate Reynolds numbers. This contrasts sharply with the sensitivity of the breakage probability on the Reynolds number, which was discussed in the previous section. Although aggregate stability in terms of breakage probability depends on the Reynolds number, their stable

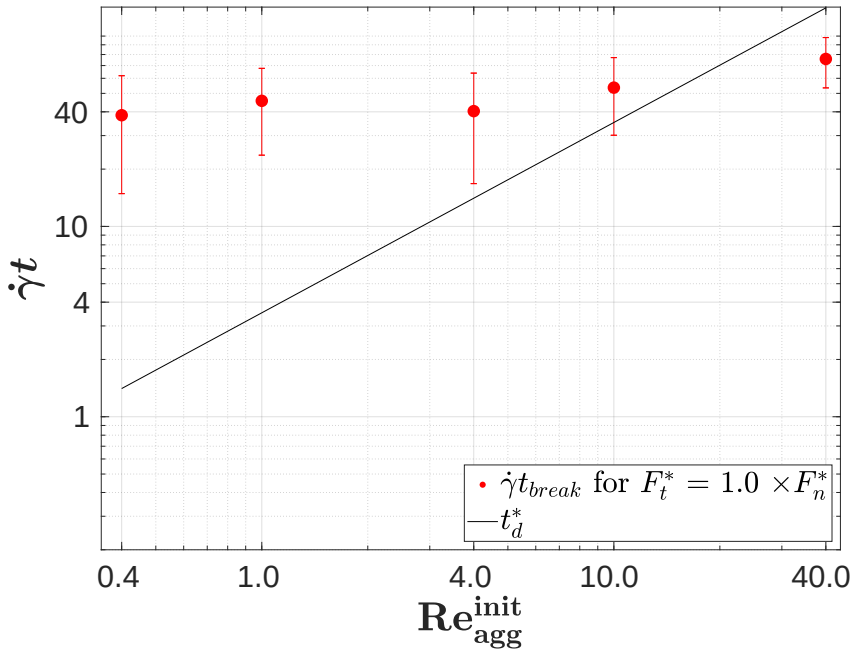


Figure 11: Dimensionless breakage time $\dot{\gamma}t_{\text{break}}$ for $F_t^* = 1.00 \times F_n^*$, plotted as a function of the Reynolds number. Also shown is the dimensionless diffusion time $t_d^*$ for the respective Reynolds number.

size and breakage kinetics do not.

Examining the effect of flow inertia in terms of aggregate breakage and restructuring may also indicate how the hydrodynamic forces are balanced through the inter-particle forces within the aggregate. Since breakage is mostly dependent on normal forces and restructuring on the bending moment,[14] it is possible that the flow inertia is competing against the normal forces to a greater extent, while having little impact on the tangential forces.

# Conclusions

While aggregate evolution in viscosity-dominated flows has been extensively investigated, the effects of finite Reynolds number were relatively unknown. Here, the dependence of aggregate evolution on Reynolds number was investigated through numerical simulations. Aggregates were characterized by their radius of gyration and the maxima of the forces responsible for the bonds between their primary particles. Such aggregates were exposed to a shear flow where shear was imposed through stresses acting on opposite

faces of the simulation domain. As aggregates evolved, their sizes and breakage rates were recorded. An analysis of aggregate stable size was conducted by tracking aggregate properties through multiple stages of their breakage cascade. Results were compared and validated against data from other studies and showed that stable size in finite Reynolds conditions is similar to negligible flow inertia conditions.

Breakage kinetics, on the other hand, are found to be significantly impacted by Reynolds number. It is found that the breakage time is not only a function of the inter-particle and hydrodynamic forces, but also of the time taken for the shear to diffuse into aggregates, which is governed by momentum diffusion. This understanding of breakage kinetics is novel, and can be taken into account in breakage kernels used in population balance equations. Specifically, when the hydrodynamic forces are high compared to the cohesive forces, breakage rate should not be considered infinitely high,[13,49] but should instead be increased progressively to capture the delayed breakage. On the other hand, when breakage is not assumed to be infinitely high, fragmentation kernels in population balance should also take into account the increase in breakage probability with aggregate Reynolds number.

At lower shear rates, momentum diffusion is fast compared to aggregate evolution and consequently does not govern aggregate breakage. However, finite Reynolds effects still play a role. An attempt was made to distinguish the effect of flow inertia on aggregate evolution from the combined effect of momentum diffusion and particle-particle interactions by scaling particle-particle interaction forces with the drag. Flow inertia was found to increase breakage probability; that is, more aggregates tend to break on increasing the Reynolds number. However, the strain at breakage is found to be the same irrespective of the Reynolds number, establishing that inertia has no significant impact on breakage kinetics for the flow conditions investigated here. Also, the final structure of the aggregates is unaffected by flow inertia.

The findings of this first-of-its-kind study expand the fundamental understanding of aggregate evolution to finite Reynolds number conditions. This will improve the accuracy of models describing aggregate morphological evolution in industrial processes by

substantially contributing to improvements of fragmentation and restructuring kernels in population balance methods. The implications of these results are important in process modelling since significant finite-Reynolds effects were observed in conditions where they were completely neglected in other studies[35,50] from which commonly used aggregate evolution kernels are extracted.

## Acknowledgement

Most High Performance Computing resources were provided by Westgrid (www.westgrid.ca) and Compute Canada (www.computecanada.ca). Complementary computing resources were provided by the EXPLOR centre hosted by the Université de Lorraine. The authors would like to acknowledge Canada's National Sciences and Engineering Research Council (NSERC) and the sponsoring companies of the NSERC Industrial Research Chair in Pipeline Transport Processes for providing the funding and resources to conduct this study.

## References

(1) Pukánszky, B.; Móczó, J. Morphology and properties of particulate filled polymers. Macromolecular Symposia. 2004; pp 115–134.

(2) Bolto, B.; Gregory, J. Organic Polyelectrolytes in Water Treatment. *Water Research* **2007**, *41*, 2301–2324.

(3) Trofa, M.; D'Avino, G. Sedimentation of fractal aggregates in shear-thinning fluids. *Applied Sciences* **2020**, *10*, 3267–3286.

(4) Laskowski, J.; Ralston, J. *Colloid Chemistry in Mineral Processing*; Elsevier, 2015.

(5) Bellot, J.-P.; Kroll-Rabotin, J.-S.; Gisselbrecht, M.; Joishi, M.; Saxena, A.; Sanders, S.; Jardy, A. Toward Better Control of Inclusion Cleanliness in a Gas Stirred Ladle Using Multiscale Numerical Modeling. *Materials* **2018**, *11*, 1179.

(6) Vaezi, F.; Sanders, R. S.; Masliyah, J. H. Flocculation Kinetics and Aggregate Structure of Kaolinite Mixtures in Laminar Tube Flow. *Journal of Colloid and Interface Science* **2011**, *355*, 96–105.

(7) Guérin, L.; Coufort-Saudejaud, C.; Liné, A.; Frances, C. Dynamics of aggregate size and shape properties under sequenced flocculation in a turbulent Taylor-Couette reactor. *Journal of colloid and interface science* **2017**, *491*, 167–178.

(8) Neelakantan, R.; Vaezi G., F.; Sanders, R. S. Effect of shear on the yield stress and aggregate structure of flocculant-dosed, concentrated kaolinite suspensions. *Minerals Engineering* **2018**, *123*, 95–103.

(9) Trofa, M.; D'Avino, G. Rheology of a dilute suspension of aggregates in shear-thinning fluids. *Micromachines* **2020**, *11*, 443–458.

(10) Seto, R.; Botet, R.; Briesen, H. Hydrodynamic Stress on Small Colloidal Aggregates in Shear Flow Using Stokesian Dynamics. *Physical Review E* **2011**, *84*, 041405.

(11) Seto, R.; Botet, R.; Auernhammer, G. K.; Briesen, H. Restructuring of Colloidal Aggregates in Shear Flow. *The European Physical Journal E* **2012**, *35*, 128.

(12) Vanni, M.; Gastaldi, A. Hydrodynamic Forces and Critical Stresses in Low-Density Aggregates under Shear Flow. *Langmuir* **2011**, *27*, 12822–12833.

(13) Harshe, Y. M.; Lattuada, M. Breakage Rate of Colloidal Aggregates in Shear Flow through Stokesian Dynamics. *Langmuir* **2012**, *28*, 283–292.

(14) Saxena, A.; Kroll-Rabotin, J.-S.; Sanders, R. S. Numerical investigation of the respective role of cohesive and hydrodynamic forces in aggregate restructuring under shear flow. *Journal of Colloid and Interface Science* **2022**, *608*, 335–365.

(15) Chen, S.; Li, S. Collision-induced breakage of agglomerates in homogeneous isotropic turbulence laden with adhesive particiles. *Journal of Fluid Mechanics* **2020**, *902*, A28.

(16) Yao, Y.; Capecelatro, J. Deagglomeration of cohesive particles by turbulence. *Journal of Fluid Mechanics* **2020**, *911*, A10.

(17) Liu, P.; Hrenya, C. M. Cluster-induced deagglomeration in dilute gravity-driven gas-solid flows of cohesive grains. *Physical Review Letters* **2018**, *121*, 238001.

(18) Sonntag, R. C.; Russel, W. B. Structure and Breakup of Flocs Subjected to Fluid Stresses: I. Shear Experiments. *Journal of Colloid and Interface Science* **1986**, *113*, 399–413.

(19) Sonntag, R. C.; Russel, W. B. Structure and Breakup of Flocs Subjected to Fluid Stresses. *Journal of Colloid and Interface Science* **1987**, *115*, 390–395.

(20) Wengeler, R.; Nirschl, H. Turbulent hydrodynamic stress induced dispersion and fragmentation of nanoscale agglomerates. *Journal of Colloid and Interface Science* **2007**, *306*, 262–273.

(21) Ehrl, L.; Soos, M.; Morbidelli, M. Dependence of Aggregate Strength, Structure, and Light Scattering Properties on Primary Particle Size under Turbulent Conditions in Stirred Tank. *Langmuir* **2008**, *24*, 3070–3081.

(22) Soos, M.; Ehrl, L.; Bäbler, M. U.; Morbidelli, M. Aggregate breakup in a contracting nozzle. *Langmuir* **2010**, *26*, 10–18.

(23) Harshe, Y. M.; Lattuada, M.; Soos, M. Experimental and Modeling Study of Breakage and Restructuring of Open and Dense Colloidal Aggregates. *Langmuir* **2011**, *27*, 5739–5752.

(24) Kim, Y.; Kim, D. Y.; Hong, J. S.; Ahn, K. H. Agglomerate Breakup of Destabilized Polystyrene Particles under a Cross-Channel Planar Extensional Flow. *Langmuir* **2018**, *34*, 11454–11463.

(25) Saha, D.; Soos, M.; Lüthi, B.; Holzner, M.; Liberzon, A.; Babler, M. U.; Kinzelbach, W. Experimental characterization of breakage rate of colloidal aggregates in axisymmetric extensional flow. *Langmuir* **2014**, *30*, 14385–14395.

(26) Saha, D.; Bäbler, M. U.; Holzner, M.; Soos, M.; Lüthi, B.; Liberzon, A.; Kinzelbach, W. Breakup of finite-size colloidal aggregates in turbulent flow investigated by three-dimensional (3D) particle tracking velocimetry. *Langmuir* **2016**, *32*, 55–65.

(27) Brady, J. F.; Bossis, G. Stokesian Dynamics. *Annual Review of Fluid Mechanics* **1988**, *20*, 111–157.

(28) Eggersdorfer, M. L.; Kadau, D.; Herrmann, H. J.; Pratsinis, S. E. Fragmentation and Restructuring of Soft-Agglomerates under Shear. *Journal of Colloid and Interface Science* **2010**, *342*, 261–268.

(29) Ruan, X.; Chen, S.; Li, S. Structural evolution and breakage of dense agglomerates in shear flow and Taylor-Green vortex. *Chemical Engineering Science* **2020**, *211*, 115261.

(30) Kroupa, M.; Vonka, M.; Soos, M.; Kosek, J. Size and Structure of Clusters Formed by Shear Induced Coagulation: Modeling by Discrete Element Method. *Langmuir* **2015**, *31*, 7727–7737.

(31) Kroll-Rabotin, J.-S.; Gisselbrecht, M.; Ott, B.; May, R.; Fröhlich, J.; Bellot, J.-P. Multiscale simulation of non-metallic inclusion aggregation in a fully resolved bubble swarm in liquid steel. *Metals* **2020**, *10*, 517.

(32) Inamuro, T.; Ii, T. Lattice Boltzmann Simulation of the Dispersion of Aggregated Particles under Shear Flows. *Mathematics and Computers in Simulation* **2006**, *72*, 141–146.

(33) Ernst, M.; Dietzel, M.; Sommerfeld, M. A lattice Boltzmann method for simulating transport and agglomeration of resolved particles. *Acta Mechanica* **2013**, *224*, 2425–2449.

(34) Saxena, A.; Kroll-Rabotin, J.-S.; Sanders, R. S. A Numerical Approach To Model Aggregate Restructuring in Shear Flow Using DEM in Lattice-Boltzmann Simulations. Progress in Applied CFD - CFD 2017. Trondheim, Norway, 2017; pp 761–772.

(35) Harshe, Y. M.; Lattuada, M. Universal Breakup of Colloidal Clusters in Simple Shear Flow. *The Journal of Physical Chemistry B* **2016**, *120*, 7244–7252.

(36) Hamaker, H. C. The London-van Der Waals Attraction between Spherical Particles. *Physica* **1937**, *4*, 1058–1072.

(37) Feke, D. L.; Prabhu, N. D.; Mann, J. A. J.; Mann, J. A. L. A Formulation of the Short-Range Repulsion between Spherical Colloidal Particles. *The Journal of Physical Chemistry* **1984**, *88*, 5735–5739.

(38) Becker, V.; Briesen, H. Tangential-Force Model for Interactions between Bonded Colloidal Particles. *Physical Review E* **2008**, *78*, 061404.

(39) Saxena, A. Aggregate Evolution in Shear Flow: Numerical Investigation of the Role of Cohesive and Hydrodynamic Forces. Ph.D. thesis, University of Alberta, 2021.

(40) Bouyer, D.; Liné, A.; Do-Quang, Z. Experimental analysis of floc size distribution under different hydrodynamics in a mixing tank. *AIChE Journal* **2004**, *50*, 2064–2081.

(41) Zaccone, A.; Soos, M.; Lattuada, M.; Wu, H.; Bäbler, M. U.; Morbidelli, M. Breakup of dense colloidal aggregates under hydrodynamic stresses. *Physical Review E* **2009**, *79*, 061401.

(42) Becker, V.; Schlauch, E.; Behr, M.; Briesen, H. Restructuring of Colloidal Aggregates in Shear Flows and Limitations of the Free-Draining Approximation. *Journal of Colloid and Interface Science* **2009**, *339*, 362–372.

(43) Zeidan, M.; Xu, B. H.; Jia, X.; Williams, R. A. Simulation of Aggregate Deformation and Breakup in Simple Shear Flows Using a Combined Continuum and Discrete Model. *Chemical Engineering Research and Design* **2007**, *85*, 1645–1654.

(44) Becker, V.; Briesen, H. A Master Curve for the Onset of Shear Induced Restructuring of Fractal Colloidal Aggregates. *Journal of Colloid and Interface Science* **2010**, *346*, 32–36.

(45) Horii, K.; Yamada, R.; Harada, S. Strength Deterioration of Nonfractal Particle Aggregates in Simple Shear Flow. *Langmuir* **2015**, *31*, 7909–7918.

(46) Vanni, M. Accurate Modelling of Flow Induced Stresses in Rigid Colloidal Aggregates. *Computer Physics Communications* **2015**, *192*, 70–90.

(47) Haddadi, H.; Morris, J. F. Topology of pair-sphere trajectories in finite inertia suspension shear flow and its effects on microstructure and rheology. *Physics of Fluids* **2015**, *27*, 043302.

(48) Mikulencak, D. R.; Morris, J. F. Stationary shear flow around fixed and free bodies at finite Reynolds number. *Journal of Fluid Mechanics* **2004**, *520*, 215.

(49) Conchúir, B. O.; Zaccone, A. Mechanism of Flow-Induced Biomolecular and Colloidal Aggregate Breakup. *Physical Review E* **2013**, *87*, 032310.

(50) Bäbler, M. U.; Biferale, L.; Brandt, L.; Feudel, U.; Guseva, K.; Lanotte, A. S.; Marchioli, C.; Picano, F.; Sardina, G.; Soldati, A.; Toschi, F. Numerical simulations of aggregate breakup in bounded and unbounded turbulent flows. *Journal of Fluid Mechanics* **2015**, *766*, 104–128.